"Gheorghe Asachi" Technical University of Iasi, Romania

BIOSORPTION OF METANIL YELLOW DYE FROM AQUEOUS SOLUTIONS BY THE ENTIRE WATER HYACINTH PLANT (*Eichhornia crassipes*) AND ITS VEGETATIVE ORGANS

Imelda Guerrero-Coronilla, Erick Aranda-García, Eliseo Cristiani-Urbina⁕

National Polytechnic Institute, National School of Biological Sciences, Biochemical Engineering Department, Wilfrido Massieu Avenue. Professional Unit Adolfo Lopez Mateos. Mexico City, 07738, Mexico

Abstract

This study explored the kinetics of metanil yellow (MY) dye biosorption onto the water hyacinth plant (*Eichhornia crassipes*) and its vegetative organs (leaves, roots, and stems). The water hyacinth's leaves exhibited the highest capacity for and initial volumetric rate of MY biosorption, followed by the entire plant, roots, and stems. Modeling the kinetics for MY biosorption onto the entire plant and vegetative organs showed that the best agreement of experimental data was achieved with the pseudo-second-order kinetic model, suggesting that the rate-determining step in the overall reaction of MY biosorption onto the biosorbents might be chemisorption. Fourier-transform infrared spectroscopy studies suggest that the amide I and II functional groups, which are present in the biosorbent proteins, participated in the biosorption of MY from aqueous solutions. A linear dependence of MY biosorption capacity at equilibrium on total protein content was observed, confirming that MY molecules bind to biosorbent proteins. Scanning electron and confocal laser scanning microscopy studies corroborated the presence of MY on the biosorbents' surface.

Key words: biosorption, *Eichhornia crassipes*, metanil yellow, pseudo-second-order kinetic

1. Introduction

Rapid technological and industrial development has exacerbated water pollution due to the accumulation of organic and inorganic compounds (Abhishek et al., 2018; Kitinya et al., 2017; Nakkeeran et al., 2018), including azo dyes. Azo dyes are the largest and most versatile class of dyes and are among the most hazardous chemical compounds in wastewaters from several industries, including textile, pharmaceutical, and cosmetics industries, among others (Padmanaban et al., 2018; Rojas-García et al., 2014; Saratale et al., 2011). Their chemical structure is characterized by the presence of one or more chromophoric azo groups (-N=N-), linked to aromatic structures containing functional groups such as -OH and –SO₃H (Rangabhashiyam et al., 2013; Rojas-

García et al., 2014). Azo dyes have serious impacts on human health (Karthik et al., 2017; Yagub et al., 2014), and their reduction products include aromatic amines, which are similarly hazardous (Saratale et al., 2011; Yagub et al., 2014). Moreover, the improper discharge of industrial wastewaters containing azo dyes into surface waters adversely affects aquatic ecosystems (Guerrero-Coronilla et al., 2015; Karthik et al., 2018; Saratale et al., 2011).

Metanil yellow (MY) dye is a highly water-soluble, anionic sulfonated monoazo dye. Its chemical formula is $C_{18}H_{14}N_3NaO_3S$, and it has a molecular weight of 375.38 g mol^{-1} (Sathya et al., 2015). This dye is widely used for the coloring of silk, wool, and leather, amongst others (Anjaneya et al., 2011; Malik, 2003; Mittal et al., 2008). Despite being a non-permitted food dye, MY is frequently used for

⁕ Author to whom all correspondence should be addressed: e-mail: ecristianiu@yahoo.com.mx; Phone: +52 5557296000 ext. 57835; Fax: +52 5557296000 ext. 46211

coloring sweet meats, ice creams, and beverages (Anjaneya et al., 2011; Mittal et al., 2008; Nath et al., 2015).

There is growing concern about the use of this dye, because it can cause serious health hazards, such as cyanosis, methemoglobinemia, neurotoxicity, carcinogenicity, and can alter the expression of genes, amongst others (Anjaneya et al., 2011; Malik, 2003; Nath et al., 2015). Therefore, the removal of MY from industrial and domestic wastewaters is crucial for protecting aquatic environments and species, as well as human health and welfare.

Nevertheless, the removal of azo dyes from water and wastewater by conventional physicochemical and biological technologies is problematic because these dyes are highly water-soluble, stable to heat, light, and oxidizing chemical agents, and recalcitrant to biodegradation due to their synthetic origin and complex aromatic structures; in addition, such technologies have significant drawbacks, including ineffective dye removal, high reagent and energy requirements, low selectivity, high capital and operating costs, low adaptability to a wide range of dye wastewaters, and/or the generation of secondary wastes that are difficult and expensive to remove or degrade (Guerrero-Coronilla et al., 2014, 2015). Biosorption technology has advantages over other technologies for treating dye-contaminated water and industrial wastewaters because of its enhanced efficacy and efficiency for removing dyes from diluted or concentrated solutions, environmental friendliness, low cost, readily available biosorbents, ease of implementation and operation, flexibility, simplicity of design, insensitivity to toxic pollutants, and lack of harmful byproducts (Gunasekar et al., 2017; Malik, 2003; Yagub et al., 2014).

The water hyacinth (*Eichhornia crassipes*, Pontederiaceae) is a freshwater, perennial, mat-forming, free-floating aquatic plant, of near worldwide distribution (Patel, 2012). Its rapid growth, ability to grow in a wide range of nutrient availability, temperatures, and pH levels, and persistence has made this species an invasive weed of increasing economic, public health, and environmental significance (Guna et al., 2017). Water hyacinth rapidly depletes nutrients and oxygen from water bodies, harbors disease-causing biological agents, threatens biodiversity, and hinders agriculture and aquaculture yields, amongst others (Guerrero-Coronilla et al., 2015; Guna et al., 2017; Patel, 2012; Sanmuga Priya and Senthamil Selvan, 2017). Water hyacinth biomass production exceeds the yield of most productive agricultural crops (Ibrahim et al., 2010), and this biomass can be used as an inexpensive, abundant, renewable, and sustainable biosorbent for removing toxic organic and inorganic pollutants from aqueous solutions (Guna et al., 2017; Mishra and Maiti, 2017).

The present study aimed to assess the biosorption potential of the entire water hyacinth plant and its vegetative organs (roots, leaves, and stems) for removing MY from aqueous solutions and to select the best one for this application. Furthermore, the key

functional groups responsible for MY biosorption onto the biosorbents were identified by Fourier transform infrared (FTIR) spectroscopy. The morphological and surface characteristics of native (MY-unloaded) and MY-loaded biosorbents were examined using scanning electron microscopy (SEM). Confocal laser scanning microscopy (CLSM) was used to visualize the presence of the MY dye on the biosorbents' surface.

2. Material and methods

2.1. Biosorbent preparation

Fresh water hyacinth plants were collected from water channels in Xochimilco, Mexico City, Mexico, and washed thoroughly with distilled deionized water. The stems, leaves, and roots were cut off and separated from some plants, while other plants were kept intact. The stems (SEC), leaves (LEC), roots (REC), and entire plants (EEC) were oven-dried separately at 60 °C until the dry weight was constant. Subsequently, they were milled using a Glen Creston hammer mill, and the resulting particles were screened using ASTM standard sieves to obtain fractions with different particle sizes. The fraction with particle sizes of 0.15-0.3 mm was used. The sieved biosorbents (SEC, LEC, REC, and EEC), without any further chemical or physical treatment, were stored in airtight plastic containers until ready for use in the MY biosorption experiments.

2.2. Chemicals

MY dye was purchased from Sigma-Aldrich® Chemicals (St. Louis, MI, USA), and the other reagents were of analytical grade (J.T. Baker®, Mexico). The molecular structure of MY is shown in Fig. 1. A 1 g L^{-1} MY stock solution was prepared by dissolving an accurately weighed amount of MY in distilled deionized water. Test MY solutions were prepared by diluting the MY stock solutions with distilled deionized water.
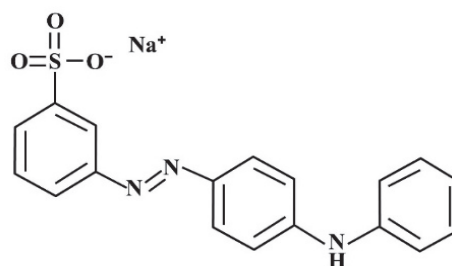

Fig. 1. Molecular structure of metanil yellow dye

2.3. Kinetic studies of MY biosorption and analytical method

Batch kinetic biosorption experiments were conducted to assess and compare the MY biosorption levels of SEC, LEC, REC, and EEC from aqueous

solutions. All the experiments were carried out in 500 mL Erlenmeyer flasks containing 120 mL 50 mg L^{-1} MY solution at pH 2.0 ± 0.1 and 1 g (dry weight) L^{-1} of biosorbent. Flasks were placed in a shaker (Cole Parmer Instrument Company, Vernon Hills, IL, USA) with a constant shaking speed of 120 rpm and a temperature of 20 ± 1°C. Throughout the course of the biosorption experiments, the pH of each solution was maintained by periodic checking and adjusting with 0.1 M HCl or NaOH solutions when necessary.

To check for glass adsorption of MY, MY photolysis, and/or MY precipitation, biosorbent-free controls were run simultaneously under the same conditions as those for the batch MY biosorption experiments. Throughout the experiments, no change in the MY concentration was detected in the controls, indicating that the observed MY removal in the biosorption experiments were due solely to the biosorbents.

At different experimental times, liquid samples were removed from the flasks, centrifuged at 3000 rpm for 5 min, and the biosorbent-free supernatants were subsequently analyzed spectrophotometrically for MY concentration at a wavelength of 434 nm using an Evolution 201 UV-visible spectrophotometer (Thermo Fisher Scientific, Whaltman, MA, USA).

The biosorption capacity of MY (q_t, mg g^{-1}) represents the amount of MY removed at time t per unit (dry weight) of biosorbent biomass, and was estimated by Eq. (1) (Lopez-Nuñez et al., 2014):

$$q_t = \frac{(C_0 - C_t)}{X} \tag{1}$$

where C_o is the initial concentration of MY (mg L^{-1}) in the aqueous phase at time $t_0 = 0$ h, C_t is the residual MY concentration (mg L^{-1}) at time $t = t$ (h), and X is the biosorbent concentration (g L^{-1}).

The volumetric MY biosorption rate (V_N, mg L^{-1} h^{-1}) was calculated by Eq. (2) (Guerrero-Coronilla et al., 2014):

$$V_N = \frac{C_0 - C_t}{t - t_0} \tag{2}$$

All the batch biosorption experiments were repeated three times, and this paper reports the mean values. MY biosorption data were statistically analyzed by a two-way analysis of variance, using Tukey's test with a 0.05 significance level. Statistical analyses were performed using GraphPad Prism software version 6.0 (GraphPad Software, Inc., La Jolla, CA, USA).

2.4. Modeling of batch biosorption kinetics

Kinetic modeling of the batch biosorption processes provides useful information on the biosorption rate, rate-controlling steps, factors affecting the biosorption rate and mechanism, and the design and optimization of biosorption facilities on a

large scale (Wahab et al., 2010). In this study, the kinetics of MY biosorption were analyzed using pseudo-first-order, pseudo-second-order, Elovich, fractional power, and intraparticle diffusion models.

Lagergren's pseudo-first-order kinetic model is expressed by Eq. (3) (Febrianto et al., 2009):

$$q_t = q_{e1}(1 - e^{-k_1 t}) \tag{3}$$

where q_t and q_{e1} are the biosorption capacities (mg g^{-1}) at any time t (h) and at equilibrium, respectively, and k_1 is the pseudo-first-order model rate constant (h^{-1}).

Ho's pseudo-second-order kinetic model is expressed by Eq. (4) (Ho and McKay, 1999):

$$q_t = \frac{t}{\frac{1}{k_2 q_{e2}^2} + \frac{t}{q_{e2}}} \tag{4}$$

where q_t is the biosorption capacity (mg g^{-1}) at any time t (h), q_{e2} is the equilibrium biosorption capacity (mg g^{-1}), and k_2 is the pseudo-second-order model rate constant (g mg^{-1} h^{-1}).

The Elovich kinetic model is expressed by Eq. (5) (Guerrero-Coronilla et al., 2014):

$$q_t = \frac{1}{\beta_e} \ln(1 + \alpha_e \beta_e) + \frac{1}{\beta_e} \ln(t) \tag{5}$$

where q_t is the biosorption capacity (mg g^{-1}) at any time t (h), β_e is the desorption constant (g mg^{-1}), and α_e is the initial biosorption rate (mg g^{-1} h^{-1}) during any one experiment.

The fractional power kinetic model is given by Eq. (6) (Guerrero-Coronilla et al., 2014):

$$q_t = k_p t^v \tag{6}$$

where: q_t is the biosorption capacity (mg g^{-1}) at time t (h), k_p is the fractional power model constant (mg g^{-1}), and v is the fractional power model rate constant (h^{-1}). The intraparticle diffusion model can be expressed by Eq. (7) (El Nemr et al., 2015):

$$q_t = k_{id} t^{0.5} + C \tag{7}$$

where q_t is the biosorption capacity (mg g^{-1}) at any time t (h), k_{id} is the intraparticle diffusion rate constant (mg g^{-1} h$^{-0.5}$), and C is the model intercept, which is related to the boundary layer thickness.

The GraphPad Prism software version 6.0 (GraphPad Software, Inc., La Jolla, CA, USA) was used to estimate all the kinetic model parameters by nonlinear regression analysis of the experimental data. The best-fit model was selected by the highest coefficient of determination (R^2), the lowest residual or sum of squared error (*SSE*), root-mean-square error (*RMSE*) or standard error values, and the narrowest 95% confidence intervals.

2.5. FTIR spectroscopy analysis

FTIR spectroscopy was used to obtain information on the main functional groups present on the surfaces of the biosorbents (SEC, LEC, REC, and EEC) and to identify possible modifications of biosorption active sites on the biosorbents during MY biosorption (Wahab et al., 2010).

Biosorbent samples (1 g L^{-1}) were mixed with 200 mg L^{-1} MY solutions at pH 2.0 for 24 h, with constant agitation at 120 rpm and 20 ± 1 °C to saturate the biosorption binding sites with MY molecules. All the suspensions were then subjected to centrifugation at 3000 rpm for 5 min, and the pellets collected were washed with distilled deionized water for removing the unbound MY molecules. The resulting suspensions were subsequently centrifuged to pellet the biosorbents biomass. Next, MY-loaded biosorbents were dried at 105 °C until the dry weight was constant in order to ensure that the biosorbents did not retain water that could interfere with the observation of hydroxyl functional groups on their surface. Finely ground MY-unloaded (native) and MY-loaded biosorbents were mixed with dried spectroscopy KBr in a 1:5 ratio. The resulting mixture was pressed with a pressure of 10 t for 2 min to yield pellets, which were analyzed by diffuse reflectance FTIR spectroscopy using a Perkin-Elmer Spectrum 2000 spectrometer. The FTIR spectra were run in the range of wavenumbers from 4000 to 400 cm^{-1} with a resolution of 4 cm^{-1} with 16 scans.

2.6. SEM analysis

To analyze the morphological features and surface characteristics of native and MY-loaded REC, SEC, LEC, and EEC, micrographs were obtained using a JEOL SEM, JSM 7800, at an accelerating voltage of 15 kV after gold coating.

2.7. CLSM analysis

The non-destructive technique of CLSM was employed to observe the presence of MY on the surface of the MY-loaded biosorbents. CLSM imaging of each MY-loaded biosorbent was performed in a Carl Zeiss LSM 710 NLO laser scanning confocal/multiphoton microscope, which is equipped with a 20×/0.8 Plan-Apochromat objective lens. The excitation wavelengths were 405, 488, 561, and 633 nm with laser powers of 35, 2.0, 2.0, and 2.0%, respectively; the detection range was 419–730 nm. The MY-loaded biosorbents were mounted on coverslips and observed directly under the confocal microscope, obtaining two-dimensional images.

3. Results and discussion

3.1. Batch biosorption kinetics of MY onto experimental biosorbents

Fig. 2 shows the variations in residual concentration, volumetric biosorption rate, and biosorption capacity of MY regarding experimental biosorption time for all the experimental biosorbents (SEC, LEC, REC, and EEC). The MY concentration in solution gradually decreased from approximately 45 mg L^{-1} to 17.5, 13.56, 10.42, and 1.86 mg L^{-1} as experimental biosorption time increased from 0 to 72 h for SEC, REC, EEC, and LEC, respectively (Fig. 2a). These results show that the entire water hyacinth plant and its vegetative organs have the capacity of biosorbing MY from aqueous solutions, but they differ significantly in their extent of biosorption ($p < 0.05$).

The volumetric MY biosorption rates of the assayed biosorbents decreased rapidly during the first 10 min of contact. The decrease was slower from 10 to 60 min, and as experimental time proceeded to 72 h, the volumetric MY biosorption rates became negligible (Fig. 2b).

These results indicate that, regardless of the biosorbent assayed, the biosorption of MY was initially rapid and gradually decreased until equilibrium was reached. The high MY biosorption rate obtained within the first minutes of contact may be due to (1) the high MY concentration in solution, which increased the driving force of the MY concentration gradient that facilitates fast transfer of MY molecules to the biosorbents' surface (Guerrero-Coronilla et al., 2015) and (2) to a large number of unoccupied biosorption binding sites on the biosorbents' surface (Lim et al., 2015). The subsequent progressive decrease in the number of vacant binding sites, together with the decreased MY concentration in solution, resulted in reduced MY biosorption rates, until the biosorption rate of MY molecules finally became zero when equilibrium was reached (Moyo et al., 2017).

The highest initial volumetric rate of MY biosorption was obtained with LEC (501.34 mg L^{-1} h^{-1}), followed by EEC (443.07 mg L^{-1} h^{-1}), REC (435.19 mg L^{-1} h^{-1}), and SEC (307.96 mg L^{-1} h^{-1}). Furthermore, Fig. 2c indicates that the MY biosorption capacity of all the assayed biosorbents increased as the experimental biosorption time increased until the biosorption capacity reached a maximum constant value that corresponded to the equilibrium biosorption capacity (q_e) value. The highest MY biosorption capacity was obtained with LEC (43.5 mg g^{-1}), followed by EEC (34.56 mg g^{-1}), REC (30.27 mg g^{-1}), and SEC (27.5 mg g^{-1}).

The contact times required to reach equilibrium ($t_{e\ exp}$) were 2, 3, 4 and 4 h for REC, SEC, LEC, and EEC, respectively (Table 1). LEC and EEC needed a longer contact time to attain equilibrium than REC and SEC did, and this may be because they biosorbed larger amounts of MY than did REC and SEC. The equilibrium biosorption times of REC, SEC, EEC, and LEC were similar to those reported for MY adsorption by Mg-Fe-NO$_3$ layered double hydroxide (Nejati et al., 2011), bottom ash, de-oiled soya (Mittal et al., 2008), and chitosan-immobilized aquatic weed (Sivashankar et al., 2013).
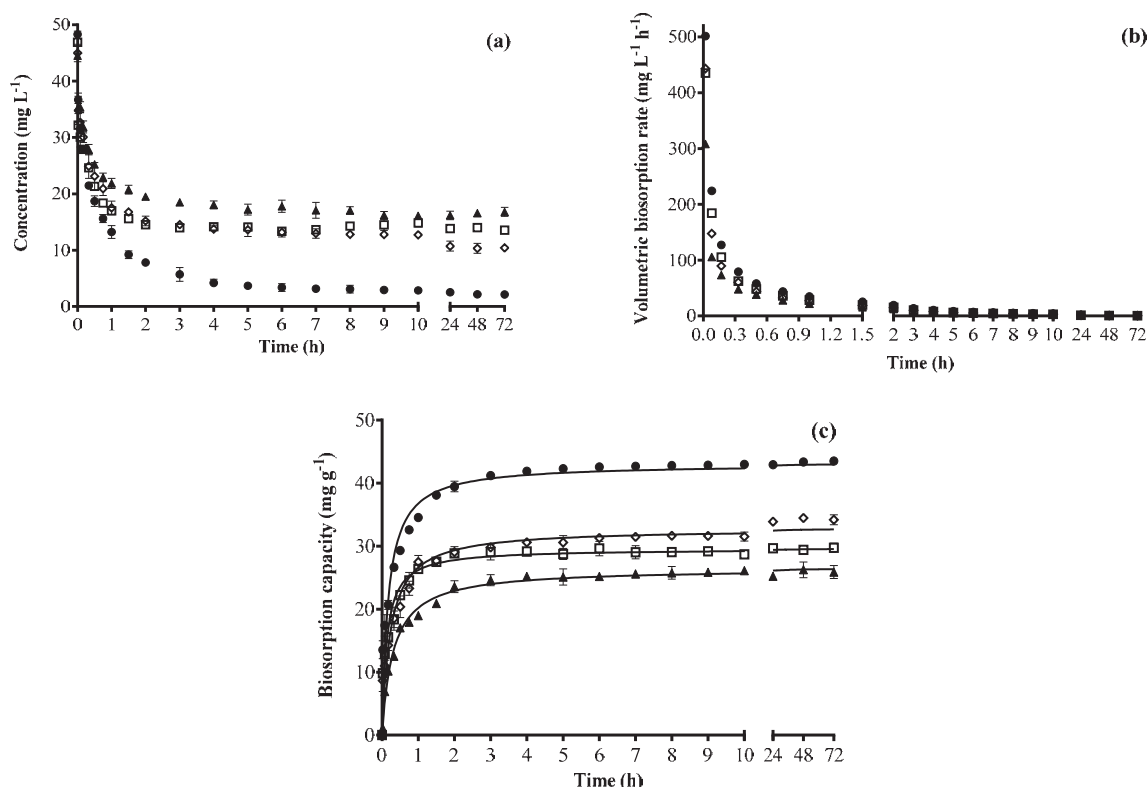
Fig. 2. Dependence of residual concentration (a), volumetric biosorption rate (b), and biosorption capacity (c) of metanil yellow on shaking contact time for the leaves (•), roots (□), and stems (▲) of *Eichhornia crassipes* as well as the whole plant (◇)

Table 1. Parameters of pseudo-first-order kinetic model for metanil yellow biosorption onto the entire *Eichhornia crassipes* plant and its vegetative organs

| Biosorbent | $t_{e\ exp}$ (h) | $q_{e\ exp}$ (mg g^{-1}) | Pseudo-first-order | | | | |
			q_{e1} (mg g^{-1})	k_1 (h^{-1})	R^2	SSE	RMSE
LEC	4	42.87 ± 0.15	41.38 ± 0.465	3.221 ± 0.217	0.899	1511	3.830
REC	2	29.66 ± 0.10	28.61 ± 0.291	4.060 ± 0.265	0.909	620.6	2.455
SEC	3	25.50 ± 0.15	25.08 ± 0.201	1.993 ± 0.084	0.965	253.2	1.568
EEC	4	34.29 ±0.16	31.24 ± 0.345	2.518 ± 0.155	0.917	787.5	2.765

EEC: entire E. crassipes plant; LEC: leaves of E. crassipes; REC: roots of E. crassipes; SEC: stems of E. crassipes; $t_{e\ exp}$: equilibrium time; k_1: pseudo-first-order model rate constant; $q_{e\ exp}$: equilibrium biosorption capacity; q_{e1}: biosorption capacity at equilibrium; R^2: coefficient of determination; RMSE: root-mean-square error; SSE: sum of squared error

It provides useful information on the efficiency and efficacy of a biosorbent to adsorb a particular adsorbate and ultimately on the potential success of the biosorbent in practical applications (Lim et al., 2015).

The above results show that water hyacinth leaves were more appropriate for MY biosorption from aqueous solutions than the roots, stems, and even the whole plant were. Similarly, water hyacinth leaves were found to be more suitable for the biosorption of amaranth azo dye from aqueous solutions, followed by the whole plant, roots, and stems (Guerrero-Coronilla et al., 2014).

Comparing different biosorption systems for the removal of a target pollutant from aqueous solutions is difficult due to diverse operating conditions used in experiments. Nonetheless, we compared the MY biosorption capacity of SEC, REC,

LEC, and EEC with that of several adsorbents reported in the literature. Results of the comparison made at similar initial MY concentrations indicate that the experimental MY biosorption capacity of LEC was similar to that reported for Mg-Fe-NO$_3$ layered double hydroxide (42.72 mg g^{-1}; Nejati et al., 2011) and significantly higher than that obtained for bottom ash (4.77 mg g^{-1}; Mittal et al., 2008), de-oiled soya (3.66 mg g^{-1}; Mittal et al., 2008), and chitosan-immobilized aquatic weed (9.91 mg g^{-1}; Sivashankar et al., 2013). Furthermore, the MY biosorption capacity of SEC, REC, and EEC was higher than that obtained for bottom ash, de-oiled soya (Mittal et al., 2008), and chitosan-immobilized aquatic weed (Sivashankar et al., 2013) but lower than that for Mg-Fe-NO$_3$ layered double hydroxide (Nejati et al., 2011). Therefore, its low cost, renewable nature, widespread availability, and effective MY biosorption make LEC an attractive

and useful biosorbent for the detoxification of MY-contaminated water and industrial wastewater.

3.2. Modeling of MY biosorption kinetics

In this study, the kinetic curves of MY biosorption onto REC, SEC, LEC, and EEC were simulated with the pseudo-first-order, pseudo-second-order, Elovich, fractional power, and intraparticle diffusion kinetic models. Tables 1-3 present the experimental values of equilibrium time ($t_{e\,exp}$) and equilibrium biosorption capacity ($q_{e\,exp}$) as well as the kinetic parameter values of the pseudo-first-order (k_1 and q_{e1}) (Table 1), pseudo-second-order (k_2 and q_{e2}), Elovich (α_e and β_e) (Table 2), fractional power (k_p and v), and intraparticle difussion (k_{id} and C) models (Table 3), along with the corresponding values of the error functions (R^2, *RMSE*, and *SSE*) applied in this study.

For all the biosorbents assayed, the pseudo-second-order kinetic model yielded the highest R^2 and the lowest *RMSE* and *SSE* values of the five tested kinetic models, indicating that MY biosorption followed pseudo-second-order kinetics. Indeed, the pseudo-second-order model successfully described the kinetic profiles of MY biosorption throughout the biosorption period (solid lines in Fig. 2c), and the predicted MY biosorption capacity values at equilibrium (q_{e2}; Table 2) were close to those determined experimentally ($q_{e\,exp}$; Table 1).

The good fit between the MY biosorption kinetics and the pseudo-second-order model suggests that the biosorption process of MY onto REC, SEC, LEC, and EEC has a chemical process (chemisorption) as the rate-controlling step (Abhishek et al., 2018; Karthik et al., 2017, 2018), involving valence forces through the exchange or sharing of electrons between the biosorbents' surface and MY molecules (Febrianto et al., 2009; Puentes-Cárdenas et al., 2012). Nejati et al.'s (2011) study on the adsorption of MY onto Mg-Fe-NO₃ layered double hydroxide also found that the biosorption process follows pseudo-second-order kinetics. Contrastingly, the MY biosorption kinetics onto bottom ash, de-oiled soya (Mittal et al., 2008), and chitosan-immobilized aquatic weed followed the

pseudo-first-order model (Sivashankar et al., 2013).

3.3. FTIR spectroscopy studies

FTIR spectroscopy studies were conducted to identify surface functional groups that are capable of biosorbing MY molecules. For this purpose, the FTIR spectra of native biosorbents were compared with those of MY-loaded biosorbents (Fig. 3). The peak positions of the major infrared (IR) absorption bands are summarized in Table 4. Fig. 3 shows that the FTIR spectra of native biosorbents displayed a number of absorption bands within the interval from 4000 to 400 cm⁻¹ wavenumbers, reflecting the complex chemical nature of the biosorbents.

FTIR spectra of native LEC, REC, SEC, and EEC biosorbents showed a broad absorption band at 3600-3000 cm⁻¹, which is attributable to the stretching vibration of -OH and -NH functional groups engaged in hydrogen bonds. This absorption band has been associated with the vibrations of the linked hydroxy groups in cellulose and lignin present in lignocellulosic materials as well as water adsorbed on their surface (Zou et al., 2013).

Water hyacinth is composed mainly of lignocellulose (cellulose, hemicellulose, and lignin), which is hygroscopic and has an affinity for water that is able to permeate the non-crystalline portion of cellulose and all of the hemicellulose and lignin (Bhattacharya et al., 2015). The -NH stretching band in the FTIR spectrum of native biosorbents also suggested the presence of amino acids (Gusain and Suthar, 2017), which are the basic units of proteins. In this respect, it has been reported that the total protein content of the leaves, stems, roots, and whole plant of water hyacinth is 33.34, 20.78, 22.26, and 25.26%, respectively (Guerrero-Coronilla et al., 2014).

Likewise, the FTIR spectra of all native biosorbents revealed a large number of absorption bands related to functional groups that are present in holocellulose, such as the C-H deformation in hemicelluloses at approximately 1320 cm⁻¹ (Manivannan and Narendhirakannan, 2015), the C-O stretching in cellulose, hemicellulose, and proteins at approximately 1420 cm⁻¹ (Gusain and Suthar, 2017).

Table 2. Parameters of pseudo-second-order and Elovich kinetic models for metanil yellow biosorption onto the entire *Eichhornia crassipes* plant and its vegetative organs

Biosorbent	Pseudo-second-order					Elovich				
	q_{e2} (mg g⁻¹)	k_2 (g mg⁻¹ h⁻¹)	R^2	SSE	RMSE	α_e (mg g⁻¹ h⁻¹)	β_e (g mg⁻¹)	R^2	SSE	RMSE
LEC	43.07 ± 0.347	0.135 ± 0.009	0.957	637.8	2.488	9201 ± 2818	0.236 ± 0.009	0.868	1146	3.420
REC	29.58 ± 0.230	0.263 ± 0.018	0.955	304.3	1.719	15916 ± 6979	0.375 ± 0.019	0.803	733.4	2.736
SEC	26.46 ± 0.138	0.122 ± 0.005	0.989	83.58	0.901	749.6 ± 171.7	0.305 ± 0.012	0.861	727.5	2.725
EEC	32.78 ± 0.278	0.129 ± 0.008	0.961	371.1	1.898	2430 ± 543.4	0.277 ± 0.009	0.901	606.8	2.488

EEC: entire E. crassipes plant; LEC: leaves of E. crassipes; REC: roots of E. crassipes; SEC: stems of E. crassipes; α_e: initial biosorption rate; β_e: desorption constant; k_2: pseudo-second-order model rate constant; q_{e2}: biosorption capacity at equilibrium; R^2: coefficient of determination; RMSE: root-mean-square error; SSE: sum of squared error

Table 3. Parameters of fractional power and intraparticle diffusion kinetic models for metanil yellow biosorption onto the entire *Eichhornia crassipes* plant and its vegetative organs

Biosorbent	Fractional power					Intraparticle diffusion				
	k_p (mg g^{-1})	v (h^{-1})	R^2	SSE	RMSE	k_{id} (mg g^{-1} h$^{-0.5}$)	C (mg g^{-1})	R^2	SSE	RMSE
LEC	32.31 ± 0.525	0.108 ± 0.007	0.776	1952	4.463	3.445 ± 0.848	26.65 ± 2.635	0.387	9133	9.417
REC	23.07 ± 0.386	0.096 ± 0.007	0.712	1073	3.310	2.145 ± 0.599	19.38 ± 1.860	0.329	4556	6.651
SEC	17.73 ± 0.459	0.139 ± 0.010	0.726	1438	3.830	2.453 ± 0.583	14.04 ± 1.805	0.404	4316	6.473
EEC	23.22 ± 0.410	0.127 ± 0.007	0.809	1164	3.446	2.880 ± 0.639	19.08 ± 2.020	0.448	4828	6.983

EEC: entire E. crassipes plant; LEC: leaves of E. crassipes; REC: roots of E. crassipes; SEC: stems of E. crassipes; k_p: fractional power model constant; k_{id}: intraparticle diffusion rate constant; v: fractional power model rate constant; C: intraparticle diffusion model intercept; R^2: coefficient of determination; RMSE: root-mean-square error; SSE: sum of squared error
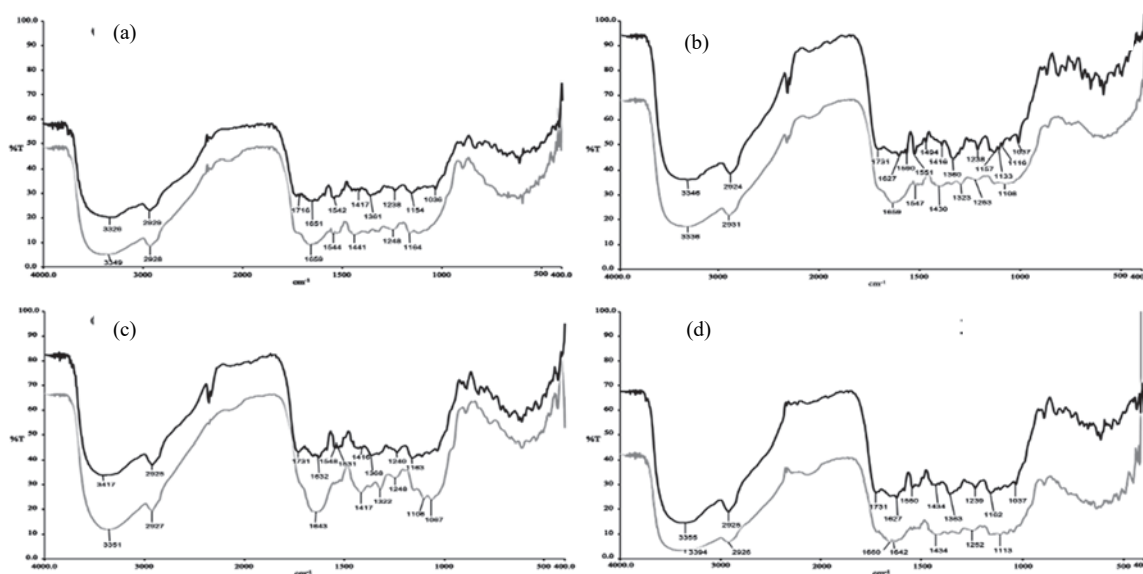

Fig. 3. Fourier transform infrared spectra of native (gray continuous lines) and metanil yellow–loaded (black continuous lines) leaves (a), roots (b), and stems (c) of *Eichhornia crassipes* as well as the entire plant (d)

Table 4. Summary of IR spectral bands for native and MY-loaded biosorbents

IR band frequency (cm^{-1})								Functional group assignment	Reference
Native biosorbents				MY-loaded biosorbents					
LEC	REC	SEC	EEC	LEC	REC	SEC	EEC		
3349	3336	3351	3394	3326	3346	3417	3355	O-H stretching N-H stretching	Zou et al. (2013) Gusain and Suthar (2017)
2928	2931	2927	2926	2929	2924	2925	2925	CH$_2$ asymmetric vibration	Zou et al. (2013)
1659	1659	1643	1642	1651	1627	1632	1627	Amide I C=O stretching	Manivannan and Narendhirakannan (2015)
1544	1547	1543	1540	1542	1590	1548	1550	Amide II N-H bending	Gusain and Suthar (2017)
1441	1430	1417	1434	1417	1416	1416	1434	C-O stretching	Gusain and Suthar (2017)
1320	1323	1322	1320	1361	1360	1368	1363	C-H deformation	Manivannan and Narendhirakannan (2015)
1248	1253	1248	1252	1238	1238	1240	1239	-SO$_3$ stretching	Wahab et al. (2010)
1164	1108	1106	1113	1154	1116	1163	1162	C-O-C vibration	Guerrero-Coronilla et al. (2014)

Also, the stretching vibration of -SO$_3$ of hemicelluloses appeared at about 1250 cm^{-1} (Wahab et al., 2010). The bands at around 1100 cm^{-1} are attributed to the vibration of C-O-C groups (Guerrero-Coronilla et al., 2014). The absorption bands of CH$_2$ asymmetric stretching vibration at approximately 2930–2920 cm^{-1}, amide I C=O stretching at around 1660–1640 cm^{-1}, and amide II N–H bending at about 1550–1540 cm^{-1} (Manivannan and Narendhirakannan, 2015; Zou et al., 2013) were also found in the FTIR spectra of all native biosorbents. The amide I and II functional groups detected in the FTIR spectra were

most likely present in water hyacinth proteins. The last portions of the spectra, which corresponded to the fingerprint region (1500–400 cm^{-1}), revealed absorption peaks that could be attributed to the vibration of metal oxides (Ibrahim et al., 2010).

The absorption spectra of MY-loaded biosorbents displayed several changes compared to those of native biosorbents. Specifically, the spectra displayed decreases in the amplitude, changes in the intensity, and/or shifting of absorption bands. These changes are indicative of interactions between MY and the functional groups present on the biosorbents' surface (Khan et al., 2012).

An important change was the decreased absorption band amplitude in the 3600–3000 cm^{-1} region, which may have resulted from a diminution in the hydrogen bonds between MY molecules and the -OH and -NH functional groups of the biosorbents; wavenumber shifts in the absorption bands of C-H, amide I C=O, and amide II N-H functional groups were also observed. According to Mishra et al. (2014), shifts in different absorption bands after biosorption are indicative of interactions between the functional groups and adsorbate. Furthermore, the relative intensity of the characteristic amide I (1660-1640 cm^{-1}) absorption bands decreased, whereas the amide II (1550-1540 cm^{-1}) bands were better defined after biosorption; these changes may indicate the involvement of amide I and II functional groups in the biosorption of MY molecules. Better-defined absorption bands were also observed at 1740–1710 cm^{-1} in the FTIR spectra of MY-loaded biosorbents, which indicate the reaction between MY molecules and the carbonyl and/or carboxyl functional groups present in some biopolymers, such as proteins and lignin (Guerrero-Coronilla et al., 2014). FTIR results indicate that hydroxyl, carbonyl, and amide functional groups participated in MY biosorption by SEC, REC, LEC, and EEC. These functional groups are present in polysaccharides, lignin, and/or proteins present in the biosorbents. We have previously reported on the chemical proximate (total ash, total protein, ether extract, crude fiber, and nitrogen-free extract) composition of the whole water hyacinth plant and its vegetative organs (Guerrero-Coronilla et al., 2014). Taking the chemical composition reported in that study and the MY biosorption capacity from the present study for each biosorbent, we discovered a linear dependence of MY biosorption capacity at equilibrium on total protein content ($R^2 = 0.97$; Fig. 4).

Contrastingly, no linear relationship was found between total ash, ether extract, nitrogen-free extract, or crude fiber and equilibrium MY biosorption capacity (data not shown). These results provide evidence that proteins play an essential role in the biosorption of MY from aqueous solutions by SEC, REC, LEC, and EEC. They also indicate that the higher the protein content of the vegetative organ or whole water hyacinth plant is, the higher the number of amide functional groups is, and, consequently, the higher the MY biosorption capacity is. Similar behavior has been reported for the biosorption of

amaranth dye by the whole water hyacinth plant and its leaves, roots, and stems (Guerrero-Coronilla et al., 2014). Moreover, it has been shown that sulfonic acid dyes, such as MY, bind to proteins in acidic solutions as a result of (1) the electrostatic attraction between the positively charged groups (e.g., amide functional groups) of proteins and the negatively charged sulfonic groups of dyes, and (2) hydrophobic interactions between the sulfonic acid dyes and the polypeptide chain backbone (Saeed et al., 2013; Tal et al., 1985).
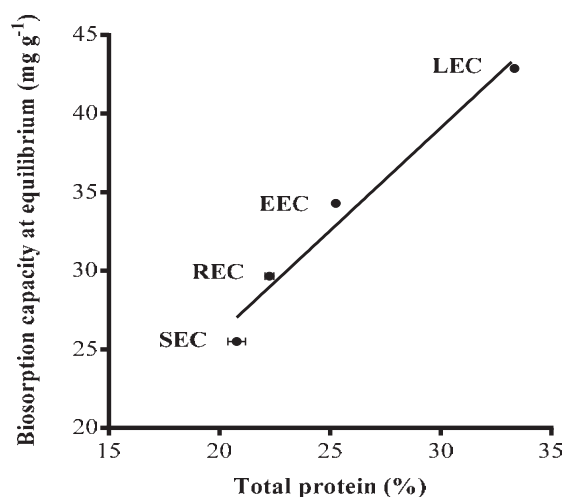

Fig. 4. Dependence of metanil yellow biosorption capacity at equilibrium on total protein content of biosorbents; EEC: entire *E. crassipes* plant; LEC: leaves of *E. crassipes*; REC: roots of *E. crassipes*; SEC: stems of *E. crassipes*

3.4. SEM studies

The physical surface morphology of the biosorbents before and after MY biosorption was evaluated by SEM micrographs. Figs. 5 and 6 display the SEM images of MY-unloaded (native) and MY-loaded biosorbents. These micrographs show that the surfaces of native LEC, REC, SEC, and EEC biosorbents had a rough, fibrous, and porous structure (Figs. 5a, 5c, 6a, and 6c), with pores of various shapes and sizes. Furthermore, the morphology of all biosorbents could facilitate the biosorption of MY due to the irregularities of their structure, enabling MY biosorption in different parts of each experimental biosorbent. After the MY biosorption process, the surface morphology of the biosorbents changed, becoming more complex, rough, and heterogeneous (Figs. 5b, 5d, 6b, and 6d). Similarly, studies have reported that the surface morphology of other biosorbents also change after the biosorption of dyes (Safa and Bhatti, 2011; Saha, 2010).

3.5 CLSM analysis

CLSM is a powerful and non-destructive optical method for visualizing the structure of biopolymer mixtures, in which optical contrast is obtained by differences in fluorescence (Van de Velde et al., 2003). The auto-fluorescence of plant cells is

mainly due to the presence of lignin and chlorophylls (De Micco and Aronne, 2007). In this study, the CLSM technique was used to confirm the presence of MY on the surface of the assayed biosorbents.

Figs. 7 and 8 show CLSM images of MY-loaded LEC (Figs. 7a-7c), REC (Figs. 7d-7f), SEC (Figs. 8a-8c), and EEC (Figs. 8d-8f). The auto-fluorescence of MY (red color; Figs. 7a, 7d, 8a, and 8d) on the surface of the biosorbents and the auto-

fluorescence of lignin and/or chlorophylls (green color; Figs. 7b, 7e, 8b, and 8e) can be observed.

Furthermore, the interactions between MY and the biosorbents' surfaces are shown in two-dimensional overlay images (Figs. 7c, 7f, 8c, and 8f), which show the combination of both auto-fluorescence emissions. These results further confirm that MY bound to the surface of all the assayed biosorbents.
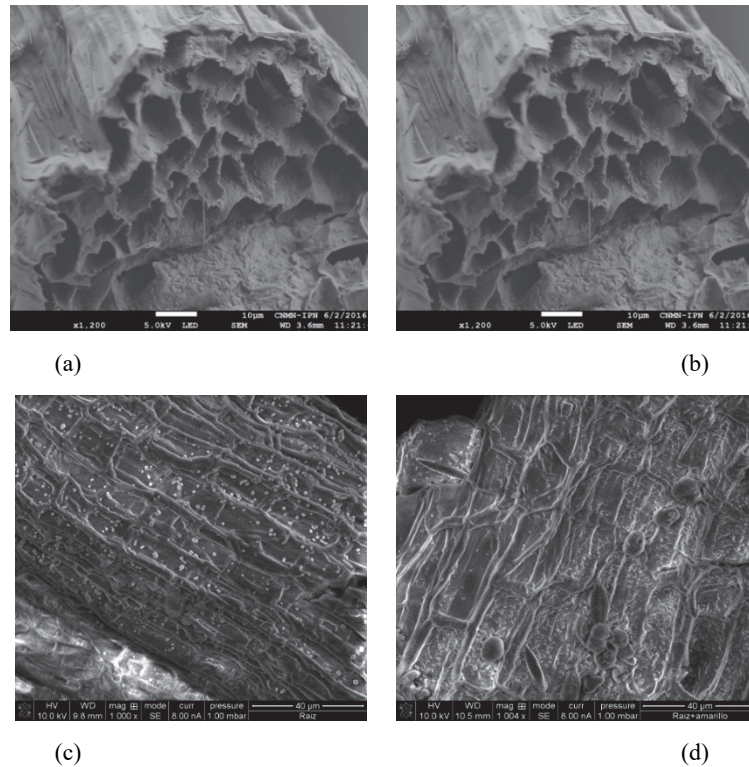

(a)   (b)

(c)   (d)

Fig. 5. Scanning electron micrographs of native (a, c) and metanil yellow–loaded (b, d) *Eichhornia crassipes* leaves (a, b) and roots (c, d)
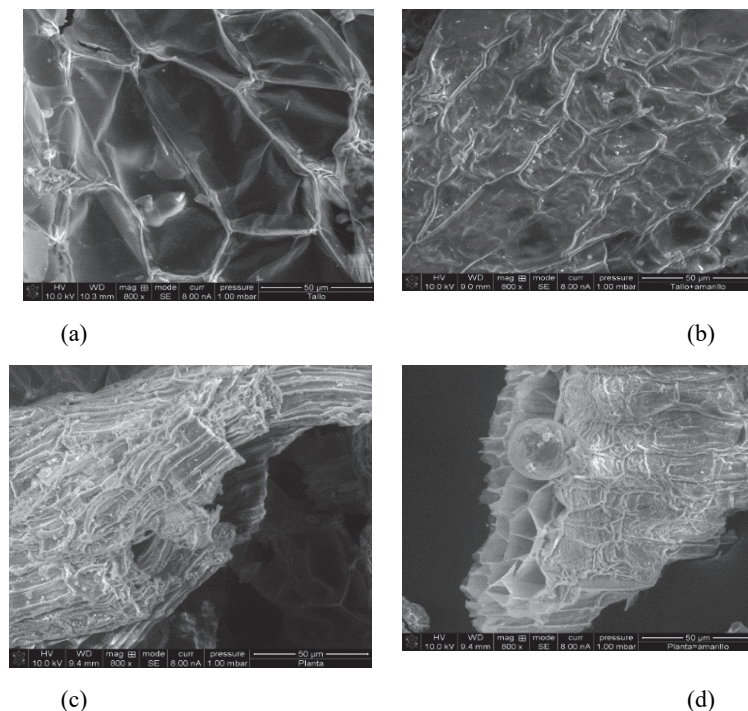

(a)   (b)

(c)   (d)

Fig. 6. Scanning electron micrographs of native (a, c) and metanil yellow–loaded (b, d) *Eichhornia crassipes* stems (a, b) as well as the entire plant (c, d)
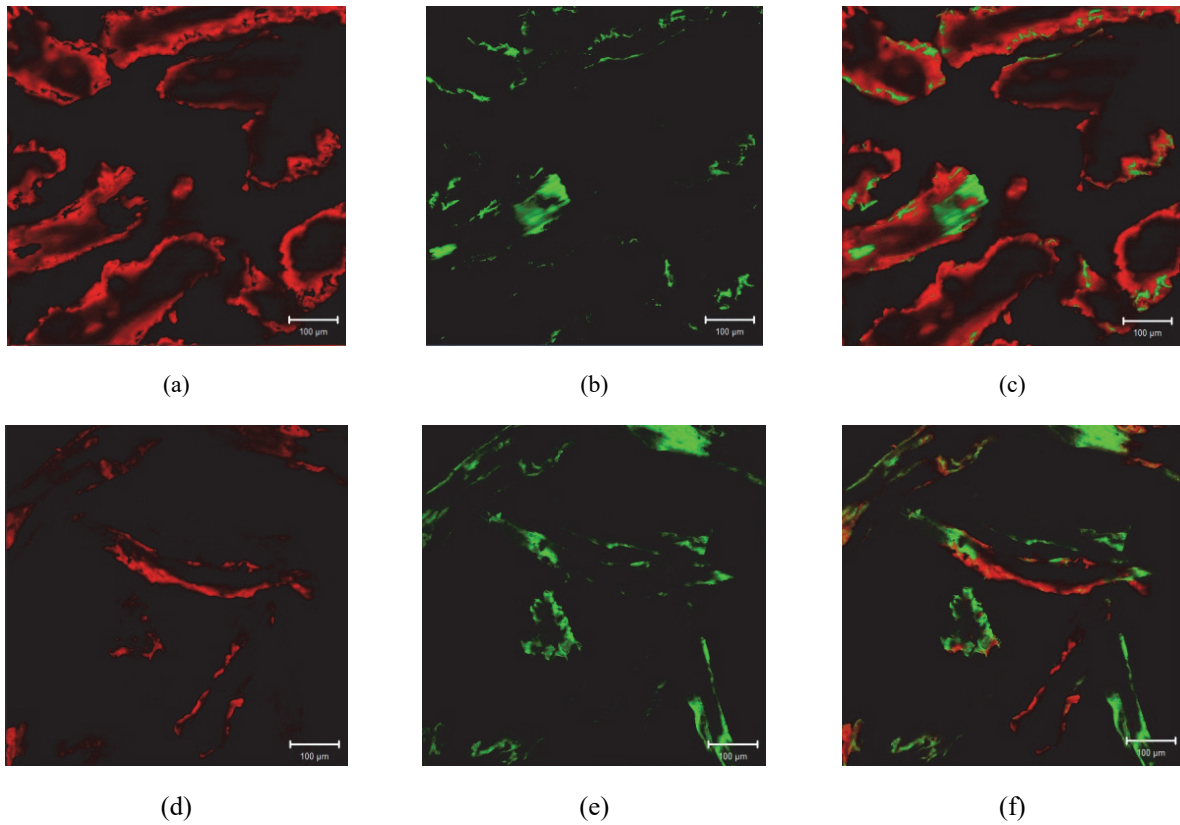
(a)   (b)   (c)

(d)   (e)   (f)

Fig. 7. Confocal laser scanning micrographs of metanil yellow (MY)-loaded *Eichhornia crassipes* leaves (a, b, c) and roots (d, e, f). Auto-fluorescence of MY is shown in red color (a, d), lignin and/or chlorophylls in green color (b, e), and interaction between the MY and biosorbents in two-dimensional overlay images (c, f).
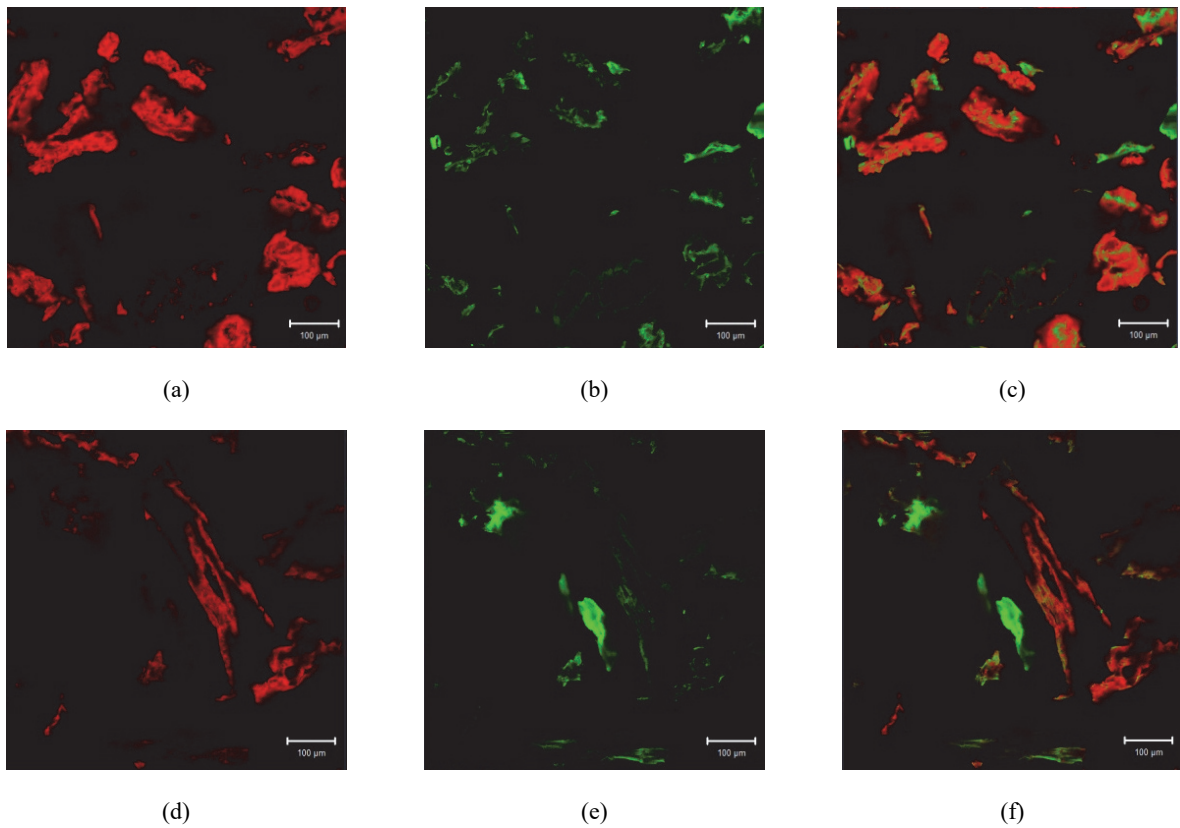

(a)   (b)   (c)

(d)   (e)   (f)

Fig. 8. Confocal laser scanning micrographs of metanil yellow (MY)-loaded *Eichhornia crassipes* stems (a, b, c) and the entire plant (d, e, f). Auto-fluorescence of MY is shown in red color (a, d), lignin and/or chlorophylls in green color (b, e), and interaction between the MY and biosorbents in two-dimensional overlay images (c, f)

4. Conclusions

The biosorption performance of the entire water hyacinth plant and its vegetative organs for removing the toxic dye MY from aqueous solutions was investigated in terms of kinetics. The best performance for biosorptive removal of MY from aqueous solutions was shown by the water hyacinth's leaves.

The biosorption kinetics of MY onto the biosorbents were described best with the pseudo-second-order model. Proteins play an essential role in the biosorption of MY by the water hyacinth. The presence of MY on the biosorbents' surface was proven by SEM and CLSM. The water hyacinth's leaves exhibited remarkable potential for application in detoxification of MY-contaminated aqueous solutions.

Acknowledgements

References

Abhishek A., Saranya N., Chandi P., Selvaraju N., (2018), Studies on the remediation of chromium (VI) from simulated wastewater using novel biomass of *Pinus kesiya* cone, *Desalination and Water Treatment*, **114**, 192-204.

Anjaneya O., Souche S.Y., Santoshkumar M., Karegoudar T.B., (2011), Decolorization of sulfonated azo dye Metanil Yellow by newly isolated bacterial strains: *Bacillus* sp. strain AK1 and *Lysinibacillus* sp. strain AK2, *Journal of Hazardous Materials*, **190**, 351-358.

Bhattacharya A., Haldar S., Chatterjee P.K., (2015), Geographical distribution and physiology of water hyacinth (*Eichhornia crassipes*) – the invasive hydrophyte and a biomass for producing xylitol, *International Journal of ChemTech Research*, **7**, 1849-1861.

De Micco V., Aronne G., (2007), Combined histochemistry and autofluorescence for identifying lignin distribution in cell walls, *Biotechnic & Histochemistry*, **82**, 209-216.

El Nemr A., El-Sikaily A., Khaled A., Abdelwahab O., (2015), Removal of toxic chromium from aqueous solution, wastewater and saline water by marine red alga *Pterocladia capillacea* and its activated carbon, *Arabian Journal of Chemistry*, **8**, 105-117.

Febrianto J., Kosasih A.N., Sunarso J., Ju Y.-H., Indraswati N., Ismadji S., (2009), Equilibrium and kinetic studies in adsorption of heavy metals using biosorbent: a summary of recent studies, *Journal of Hazardous Materials*, **162**, 616-645.

Guerrero-Coronilla I., Morales-Barrera L., Cristiani-Urbina E., (2015), Kinetic, isotherm and thermodynamic studies of amaranth dye biosorption from aqueous solution onto water hyacinth leaves, *Journal of Environmental Management*, **152**, 99-108.

Guerrero-Coronilla I., Morales-Barrera L., Villegas-Garrido T.L., Cristiani-Urbina E., (2014), Biosorption of amaranth dye from aqueous solution by roots, leaves, stems and the whole plant of *E. crassipes*, *Environmental Engineering and Management Journal*, **13**, 1917-1926.

Guna V., Ilangovan M., Anantha Prasad M.G., Reddy N., (2017), Water hyacinth: a unique source for sustainable materials and products, *ACS Sustainable Chemistry & Engineering*, **5**, 4478-4490.

Gunasekar V., Ramadoss G., Ponnusami V., (2017), Influence of process variables on adsorption of Congo red onto mango leaf char using factorial design analysis, *Environmental Engineering and Management Journal*, **16**, 2745-2753.

Gusain R., Suthar S., (2017), Potential of aquatic weeds (*Lemna gibba*, *Lemna minor*, *Pistia stratiotes* and *Eichhornia* sp.) in biofuel production, *Process Safety and Environmental Protection*, **109**, 233-241.

Ho Y.S., McKay G., (1999), Pseudo-second order model for sorption processes, *Process Biochemistry*, **34**, 451-465.

Ibrahim M., Mahani R., Osman O., Scheytt T., (2010), Effect of physical and chemical treatments on the electrical and structural properties of water hyacinth, *The Open Spectroscopy Journal*, **4**, 32-40.

Karthik V., Saravanan K., Nakkeeran E., Selvaraju N., (2017), Biosorption of turquoise blue dye from aqueous solution by dried fungal biomass (*Trichoderma harzianum*) – kinetic, isotherm and thermodynamic studies, *Desalination and Water Treatment*, **74**, 362-370.

Karthik V., Saravanan K., Patra C., Ushadevi B., Vairam S., Selvaraju N., (2018), Biosorption of acid yellow 12 from simulated wastewater by non-viable *T. harzianum*: kinetics, isotherm and thermodynamic studies, *International Journal of Environmental Science and Technology*, doi: 10.1007/s13762-018-2073-4.

Khan M.A., Ngabura M., Choong T.S.Y., Masood H., Chuah L.A., (2012), Biosorption and desorption of nickel on oil cake: batch and column studies, *Bioresource Technology*, **103**, 35-42.

Kitinya J., Onyango M., Ochieng A., (2017), Removal of multilan red and multi-active blue dyes from aqueous solution by adsorption and oxidation techniques: equilibrium, kinetics and thermodynamic studies, *Environmental Engineering and Management Journal*, **16**, 2731-2743.

Lim L.B.L., Priyantha N., Hakimah N., Mansor N.H.M., (2015), *Artocarpus altilis* (breadfruit) skin as a potential low-cost biosorbent for the removal of crystal violet dye: equilibrium, thermodynamics and kinetics studies, *Environmental Earth Sciences*, **73**, 3239-3247.

Lopez-Nuñez P.V., Aranda-García E., Cristiani-Urbina M.D.C., Morales-Barrera L., Cristiani-Urbina E., (2014), Removal of hexavalent and total chromium from aqueous solutions by plum (*P. domestica* L.) tree bark, *Environmental Engineering and Management Journal*, **13**, 1927-1938.

Malik P.K., (2003), Use of activated carbons prepared from sawdust and rice-husk for adsorption of acid dyes: a case study of Acid Yellow 36, *Dyes and Pigments*, **56**, 239-249.

Manivannan A., Narendhirakannan R.T., (2015), Bioethanol production from aquatic weed water hyacinth (*Eichhornia crassipes*) by yeast fermentation, *Waste and Biomass Valorization*, **6**, 209-216.

Mishra A., Tripathi B.D., Rai A.K., (2014), Biosorption of Cr(VI) and Ni(II) onto *Hydrilla verticillata* dried biomass, *Ecological Engineering*, **73**, 713-723.

Mishra S., Maiti A., (2017), The efficiency of *Eichhornia crassipes* in the removal of organic and inorganic pollutants from wastewater: a review, *Environmental Science and Pollution Research*, **24**, 7921-7937.

Mittal A., Gupta V.K., Malviya A., Mittal J., (2008), Process development for the batch and bulk removal and recovery of a hazardous, water-soluble azo dye (metanil yellow) by adsorption over waste materials (bottom ash and de-oiled soya), *Journal of Hazardous Materials*, **151**, 821-832.

Moyo M., Pakade V.E., Modise S.J., (2017), Biosorption of lead(II) by chemically modified *Mangifera indica* seed shells: adsorbent preparation, characterization and performance assessment, *Process Safety and Environmental Protection*, **111**, 40-51.

Nakkeeran E., Patra C., Shahnaz T., Rangabhashiyam S., Selvaraju N., (2018), Continuous biosorption assessment for the removal of hexavalent chromium from aqueous solutions using *Strychnos nux vomica* fruit shell, *Bioresource Technology Reports*, **3**, 256-260.

Nath P.P., Sarkar K., Tarafder P., Mondal M., Das K., Paul G., (2015), Practice of using metanil yellow as food colour to process food in unorganized sector of West Bengal – a case study, *International Food Research Journal*, **22**, 1424-1428.

Nejati K., Rezvani Z., Mansurfar M., Mirzaee A., Mahkam M., (2011), Adsorption of metanil yellow azoic dye from aqueous solution onto Mg-Fe-NO$_3$ layered double hydroxide, *Zeitschrift für Anorganische und Allgemeine Chemie*, **637**, 1573-1579.

Padmanaban V.C., Selvaraju N., Vasudevan V.N., Achary A., (2018), Augmented radiolytic (^{60}Co γ) degradation of direct red 80 (Polyazo dye): optimization, reaction kinetics & G-value interpretation, *Reaction Kinetics, Mechanisms and Catalysis*, **125**, 433-447.

Patel S., (2012), Threats, management and envisaged utilizations of aquatic weed *Eichhornia crassipes*: an overview, *Reviews in Environmental Science and Bio/Technology*, **11**, 249-259.

Puentes-Cárdenas I.J., Pedroza-Rodríguez A.M., Navarrete-López M., Villegas-Garrido T.L., Cristiani-Urbina E., (2012), Biosorption of trivalent chromium from aqueous solutions by *Pleurotus ostreatus* biomass, *Environmental Engineering & Management Journal*, **11**, 1741-1752.

Rangabhashiyam S., Anu N., Selvaraju N., (2013), Sequestration of dye from textile industry wastewater using agricultural waste products as adsorbents, *Journal of Environmental Chemical Engineering*, **1**, 629-641.

Rojas-García E., López-Medina R., May-Lozano M., Hernández-Pérez I., Valero M.J., Maubert-Franco A.M., (2014), Adsorption of azo-dye Orange II from aqueous solutions using a metal-organic framework material: iron-benzenetricarboxylate, *Materials*, **7**, 8037-8057.

Saeed S.M.G., Sayeed S.A., Ashraf S., Qureshi A., Ali R., Kausar R., Saify Z.S., (2013), Amaranth-protein interaction in food system and its impact on tryptic digestibility, *Journal of the Chemical Society of Pakistan*, **35**, 823-827.

Safa Y., Bhatti H.N., (2011), Adsorptive removal of direct textile dyes by low cost agricultural waste: application of factorial design analysis, *Chemical Engineering Journal*, **167**, 35-41.

Saha P., (2010), Assessment on the removal of methylene blue dye using tamarind fruit shell as biosorbent, *Water, Air, & Soil Pollution*, **213**, 287-299.

Sanmuga Priya E., Senthamil Selvan P., (2017), Water hyacinth (*Eichhornia crassipes*) - an efficient and economic adsorbent for textile effluent treatment - a review, *Arabian Journal of Chemistry*, **10**, S3548-S3558.

Saratale R.G., Saratale G.D., Chang J.S., Govindwar S.P., (2011), Bacterial decolorization and degradation of azo dyes: a review, *Journal of the Taiwan Institute of Chemical Engineers*, **42**, 138-157.

Sathya M., Elumalai S., Muthuraman G., (2015), Removal of Acid Yellow 36 from aqueous solution by solvent extraction method using tri-octyl amine as a carrier, *International Journal of ChemTech Research*, **7**, 3014-3019.

Sivashankar R., Sivasubramanian V., Sathya A.B., Pallipad S., (2013), Biosorption of hazardous azo dye metanil yellow using immobilized aquatic weed, *Proceedings of the International Conference on Future Trends in Structural, Civil, Environmental and Mechanical Engineering – FTSCEM 2013*, 153-157.

Tal M., Silberstein A., Nusser E., (1985), Why does Coomassie Brilliant Blue R interact differently with different proteins? A partial answer, *The Journal of Biological Chemistry*, **260**, 9976-9980.

Van de Velde F., Weinbreck F., Edelman M.W., Van der Linden E., Tromp R.H., (2003), Visualisation of biopolymer mixtures using confocal scanning laser microscopy (CSLM) and covalent labelling techniques, *Colloids and Surfaces B: Biointerfaces*, **31**, 159-168.

Wahab M.A., Jellali S., Jedidi N., (2010), Ammonium biosorption onto sawdust: FTIR analysis, kinetics and adsorption isotherms modeling, *Bioresource Technology*, **101**, 5070-5075.

Yagub M.T., Sen T.K., Afroze S., Ang H.M., (2014), Dye and its removal from aqueous solution by adsorption: a review, *Advances in Colloid and Interface Science*, **209**, 172-184.

Zou W., Bai H., Gao S., Li K., (2013), Characterization of modified sawdust, kinetic and equilibrium study about methylene blue adsorption in batch mode, *Korean Journal of Chemical Engineering*, **30**, 111-122.